Buckling Analysis of General Composite Laminates by Hybrid-Stress Finite Element Method

Wen-Hwa Chen* and Shau-Hwa Yang†
National Tsing Hua University, Hsinchu, Taiwan 30043, Republic of China

Without using the composite shear correction factors, an assumed hybrid-stress finite element model together with a composite multilayer element are developed to study the buckling of generally laminated composite plates with arbitrary thickness and edge conditions under an in-plane stress system. The assumed stress field satisfies 1) the equilibrium conditions within each layer, 2) the interlaminar traction reciprocity conditions, and 3) stress-free boundary conditions on the top and bottom surfaces of the laminate. The initial-stress stiffness matrix for buckling analysis is constructed by the stresses obtained from three-dimensional interlaminar stress analysis. Some numerical examples are carried out. The buckling mode shapes for various edge conditions are also demonstrated. Excellent agreements between the present results and referenced solutions show the high accuracy and validity of the present technique.

Nomenclature

A = matrix form of constraint condition on the parameters β
a,b,h = length, width, and total thickness of laminate
E_L,E_T = elastic moduli of individual layer in longitudinal and transverse directions
G_{LT},G_{TT} = shear moduli of individual layer
K^n = the bending stiffness matrix of the nth element
K_σ^n = the initial-stress stiffness matrix of the nth element
L^i,N_0^i,N_1^i,N_2^i = interpolation matrices
L,T = longitudinal and transverse direction of the lamina
$\boldsymbol{q}^i$ = generalized nodal displacements for the ith layer
S^i = the compliance matrix of the ith layer
$S_{\sigma_n}^i$ = the part of ∂v_n^i where tractions $\bar{\boldsymbol{T}}^{0^i}$ or $\bar{\boldsymbol{T}}^i$ are prescribed
$\bar{\boldsymbol{T}}^{0^i}$ = the prescribed tractions at $S_{\sigma_n}^i$ of the ith layer before the occurrence of buckling
$\bar{\boldsymbol{T}}^i$ = the prescribed tractions at $S_{\sigma_n}^i$ of the ith layer at the occurrence of buckling
$\hat{\boldsymbol{T}}^{0^i}$ = the boundary tractions at the interelement boundary for the ith layer before the occurrence of buckling
$\boldsymbol{T}^i$ = the boundary tractions for the ith layer at the occurrence of buckling
$\boldsymbol{T}^{*i}$ = incremental boundary tractions for the ith layer at the occurrence of buckling
$\bar{T}$ = dimensionless buckling load
$\boldsymbol{u}^{0^i}$ = the interelement boundary displacements of the ith layer before the occurrence of buckling
$\boldsymbol{u}^i$ = the interelement boundary displacements of the ith layer measured from the state just prior to the occurrence of buckling
v_n^i = the volume of the ith layer within the nth element
∂v_n^i = the boundary of v_n^i
$w^i,w^i_{,x},w^i_{,y}$ = the component of $\boldsymbol{u}^i$ in z direction and its corresponding partial derivatives
x,y,z = Cartesian coordinates
α,β = undetermined independent parameters
λ = Lagrangian multiplier
μ = eigenvalue
ν_{LT},ν_{TT} = Poisson's ratios
ξ,ζ,η = nondimensional local coordinates
$\overset{0}{\pi}_{HS},\pi_{HS}$ = the assumed hybrid-stress functional for interlaminar stress analysis and buckling analysis, respectively
$\hat{\boldsymbol{\sigma}}^{0^i}$ = three-dimensional stresses in the ith layer before the occurrence of buckling
$\boldsymbol{\sigma}^{0^i}$ = three-dimensional stresses in the ith layer at the state just prior to the occurrence of buckling
$\boldsymbol{\sigma}^i$ = three-dimensional stresses in the ith layer at the occurrence of buckling
$\boldsymbol{\sigma}^{*i}$ = incremental stresses in the ith layer at the occurrence of buckling

I. Introduction

THE buckling of composite laminates has been investigated intensively for some years because of its significant characteristics in engineering applications, especially in the design of aircraft structures. Hence, an accurate calculation of the critical buckling load of composite laminates is required in assessing the strength of composite structures.

The laminate plate theory is usually extended from classical plate theory (CPT) or Reissner-Mindlin shear-deformation plate theory. The classical plate theory ignores the transverse shear stresses and usually overestimates the buckling load. The Reissner-Mindlin shear-deformation plate theory corrects the Kirchhoff hypothesis and incorporates transverse shear-deformation effects. Noor[1] showed that first-order shear-deformation plate theory provides a reliable model for predicting the buckling load of thin or moderately thick plates once the composite shear correction factors are properly selected. Based on the reduced plate stiffnesses as well as shear-correction factors, Turvey[2] analyzed the biaxial buckling of moderately thick laminated plates. The methods proposed by Noor[1] and Turvey[2] are difficult to employ for laminates with arbitrary edge conditions. Recently, Reddy and Phan[3] and Putcha and Reddy[4] used a higher-order shear-deformation theory[5] to predict the buckling load. Again, the survey of the previous stud-

Received Sept. 1, 1989; revision received Feb. 19, 1990.

*Professor, Department of Power Mechanical Engineering.
†Graduate Student, Department of Power Mechanical Engineering.

ies[1-4] were restricted to the cases with simply supported edge conditions.

For the case with arbitrary edge conditions, based on the refined higher-order theories,[5,6] Khdeir and Librescu[7] and Khdeir[8] investigated the buckling of symmetric cross-ply laminated plates having one pair of opposite edges simply supported. Singh and Sadasiva Rao[9] used the displacement finite element method to analyze the stability of thick angle-ply composite plates. The method in Ref. 9 employed the shear-correction factors and was not suitable for free-edge conditions. Dawe and Craig[10] and Whitney[11] analyzed the buckling of symmetrically laminated plates subjected to in-plane stresses. However, the use of composite shear-correction factors is still required. Neglecting the transverse shear-deformation effects, Baharlou and Leissa[12] extended the Ritz method to analyze the buckling of generally laminated composite plates. Unfortunately, this method was applicable only for thin plates with simple geometry.

The aim of this work is thus to develop an accurate finite element technique without using the composite shear-correction factors for predicting the critical buckling load of generally laminated composite plates with arbitrary edge conditions under an in-plane stress system. The thickness of the laminated plate can be thin, moderately thick, or thick. The buckling analysis consists of two parts: the first part is the calculation of three-dimensional interlaminar stresses of the composite laminates before buckling occurs, and the second part is the estimation of buckling load. To calculate the three-dimensional interlaminar stresses and then buckling load accurately, the hybrid-stress finite element method seems to be a good choice.[13] Therefore, for interlaminar stress analysis, the hybrid-stress finite element model and the composite multilayer element devised in Chen and Hung[13] are adopted and modified here. However, based on the principle of complementary virtual work, a new hybrid-stress finite element model is reformulated for buckling analysis. The composite multilayer element is taken as that used for interlaminar stress analysis. Hence, the three-dimensional interlaminar stress states including transverse normal and shear stresses are all accounted for. The interlayer traction reciprocity conditions and stress-free boundary conditions on the top and bottom surfaces of the laminate are satisfied and the individual cross-sectional rotations of each layer are allowed.

To demonstrate the validity and accuracy of the present technique as developed, two different composite laminates with specific edge conditions are first solved. These include 1) symmetric cross-ply laminated plate subjected to uniaxial or biaxial compression stress having one pair of opposite edges simply supported, and 2) antisymmetric angle-ply laminated plate subjected to uniaxial compression stress with pin supports. The laminates with arbitrary edge conditions under various in-plane stresses are then studied. The buckling mode shapes for various cases are also presented. Comparisons of the calculated critical buckling loads with referenced solutions show the high accuracy and applicability of this work.

II. Hybrid-Stress Finite Element Formulations

The assumed hybrid-stress finite element model is formulated based on a modified complementary energy principle. To relax the equilibrium of interelement tractions, in addition to the stress field in the interior of the element, Lagrangian multipliers, which are physically the interelement boundary displacements, are introduced. However, it can be shown that the interelement-traction reciprocity and mechanical boundary conditions are still satisfied.[14] The details of the formulations of the interlaminar stress analysis and buckling analysis, respectively, are discussed as follows.

A. Interlaminar Stress Analysis

Assume the laminate consists of k layers and let the planar domain of the laminate be divided into m elements. The assumed hybrid-stress functional governed by the modified complementary energy principle, say, π^0_{HS}, can be written as (ignoring body forces)[13]

$$\pi^0_{HS}(\hat{\boldsymbol{\sigma}}^{0^i};\boldsymbol{u}^{0^i}) = \sum_{n=1}^{m}\left[\sum_{i=1}^{k}\left(\frac{1}{2}\int_{v_n^i}\hat{\boldsymbol{\sigma}}^{0^{i\gamma}}S^i\hat{\boldsymbol{\sigma}}^{0^i}\,\mathrm{d}v - \int_{\partial v_n^i}\hat{\boldsymbol{T}}^{0^{i\gamma}}\boldsymbol{u}^{0^i}\,\mathrm{d}s + \int_{S^i_{\sigma_n}}\bar{\boldsymbol{T}}^{0^{i\gamma}}\boldsymbol{u}^{0^i}\,\mathrm{d}s\right)\right] = \min \tag{1}$$

where $\boldsymbol{\sigma}^{0^i}$ is the vector (6×1) of three-dimensional stresses in the ith layer before the occurrence of buckling and satisfies the equilibrium conditions within each layer and the interlaminar traction reciprocity conditions. The term S^i is the compliance matrix of the ith layer, $\boldsymbol{u}^{0^i}$ is the Lagrangian multipliers and can be shown as the vector of interelement boundary displacements of the ith layer before the occurrence of buckling. The $\boldsymbol{u}^{0^i}$ is introduced to enforce the interelement traction reciprocity. The boundary tractions at the interelement boundaries for the ith layer, $\hat{\boldsymbol{T}}^{0^i}$, is derived from the assumed $\hat{\boldsymbol{\sigma}}^{0^i}$. The $\bar{\boldsymbol{T}}^{0^i}$ are the prescribed tractions at $S^i_{\sigma_n}$ of the ith layer before buckling occurs, v^i_n is the volume of the ith layer within the nth element and ∂v^i_n is the boundary of v^i_n. The $S^i_{\sigma_n}$ is the part of ∂v^i_n where tractions $\bar{\boldsymbol{T}}^{0^i}$ are prescribed. The terms $\hat{\boldsymbol{\sigma}}^{0^{i\gamma}}$, $\hat{\boldsymbol{T}}^{0^{i\gamma}}$, and $\bar{\boldsymbol{T}}^{0^{i\gamma}}$ are the transpose of $\hat{\boldsymbol{\sigma}}^{0^i}$, $\hat{\boldsymbol{T}}^{0^i}$, and $\bar{\boldsymbol{T}}^{0^i}$, respectively.

The hybrid-stress finite element models adopted in this work are characterized by an assumed stress field in the element and an assumed displacement field along the interelement boundary. The interelement boundary displacements before the occurrence of buckling, $\boldsymbol{u}^{0^i}$, for the ith layer of the nth element can be uniquely expressed in terms of the generalized nodal displacements $\boldsymbol{q}^i$ as

$$\boldsymbol{u}^{0^i} = L^i\boldsymbol{q}^i \tag{2}$$

such that the interelement displacement continuity is maintained. From the generalized Hook's law, since the in-plane strains for the ith layer of the nth element can be independently assumed in terms of undetermined parameters $\boldsymbol{\beta}$, the in-plane stresses in the ith layer can be also expressed in terms of parameters $\boldsymbol{\beta}$.

The normal stress $\hat{\sigma}^0_{zz}$ and transverse shear stresses, $\hat{\sigma}^0_{xz}$ and $\hat{\sigma}^0_{yz}$, can be obtained from equilibrium equations (ignoring body forces) as

$$\hat{\sigma}^{0^i}_{xz} = -\int\left(\hat{\sigma}^{0^i}_{xx,x} + \hat{\sigma}^{0^i}_{xy,y}\right)\mathrm{d}z \tag{3}$$

$$\hat{\sigma}^{0^i}_{yz} = -\int\left(\hat{\sigma}^{0^i}_{yx,x} + \hat{\sigma}^{0^i}_{yy,y}\right)\mathrm{d}z \tag{4}$$

$$\hat{\sigma}^{0^i}_{zz} = -\int\left(\hat{\sigma}^{0^i}_{zx,x} + \hat{\sigma}^{0^i}_{zy,y}\right)\mathrm{d}z \tag{5}$$

The constants of integration can be chosen such that the traction reciprocity conditions at the interlaminar interfaces and the free conditions on the bottom surface of the laminate are satisfied exactly. From the assumptions of in-plane strains (will be discussed in next section) and Eqs. (3-5), one can express the three-dimensional stresses $\hat{\boldsymbol{\sigma}}^{0^i}$ in the ith layer of the nth element in terms of parameters $\boldsymbol{\beta}$ as

$$\hat{\boldsymbol{\sigma}}^{0^i} = N^i_0\boldsymbol{\beta} \tag{6}$$

where N^i_0 denotes the interpolation function. The boundary tractions $\hat{\boldsymbol{T}}^{0^i}$ can be then derived from $\hat{\boldsymbol{\sigma}}^{0^i}$ and shown as

$$\hat{\boldsymbol{T}}^{0^i} = R^i_0\boldsymbol{\beta} \tag{7}$$

Substituting Eqs. (2), (6), and (7) into Eq. (1), the functional

π^0_{HS} can be formulated as

$$\pi^0_{HS}(\beta,q^i)=\sum_{n=1}^{m}\left[\sum_{i=1}^{k}\left(\frac{1}{2}\beta^\gamma H^i_0\beta-\beta^\gamma G^i_0 q^i+F^{i\gamma}_0 q^i\right)\right] \tag{8}$$

where

$$H^i_0=\int_{v^i_n} N^{i\gamma}_0 S^i N^i_0\,\mathrm{d}v$$

$$G^i_0=\int_{\partial v^i_n} R^{i\gamma}_0 L^i\,\mathrm{d}s$$

$$F^{i\gamma}_0=\int_{S^i_{\sigma_n}} \bar{T}^{0i} L^i\,\mathrm{d}s$$

After assembling the parameters in Eq. (8) for all layers, π^0_{HS} is found to be

$$\pi^0_{HS}(\beta,q^n)=\sum_{n=1}^{m}\left[\tfrac{1}{2}\beta^\gamma H^n_0\beta-\beta^\gamma G^n_0 q^n+F^{n\gamma}_0 q^n\right] \tag{9}$$

where H^n_0, G^n_0, F^n_0, and q^n are the corresponding assembled element matrices of H^i_0, G^i_0, F^i_0, and q^i $(i=1,2,\cdots k)$.

Since the transverse shear stresses are also assumed as free on the top surface of the laminate, the following condition is enforced as a constraint condition on the parameters, β, say,

$$A\beta=\mathbf{0} \tag{10}$$

and needs to be introduced into Eq. (9) by the Lagrangian multiplier λ as

$$\pi^0_{HS}(\beta,q^n,\lambda)=\sum_{n=1}^{m}\left[\tfrac{1}{2}\beta^\gamma H^n_0\beta-\beta^\gamma G^n_0 q^n+F^{n\gamma}_0 q^n+\lambda^\gamma A\beta\right] \tag{11}$$

The stationary condition of the functional π^0_{HS} in Eq. (11) with respect to β yields the relation:

$$\beta=H^{n^{-1}}_0 G^n_0 q^n-H^{n^{-1}}_0 A^\gamma\lambda \tag{12}$$

Substituting Eq. (12) into Eq. (10), the Lagrangian multiplier λ and parameter β can be thus obtained in terms of the generalized nodal displacements q^n:

$$\lambda=\left(AH^{n^{-1}}_0 A^\gamma\right)^{-1}\left(AH^{n^{-1}}_0 G^n_0\right)q^n \tag{13}$$

and

$$\beta=\left(H^{n^{-1}}_0-H^{n^{-1}}_0 A^\gamma\left(AH^{n^{-1}}_0 A^\gamma\right)^{-1}AH^{n^{-1}}_0\right)G^n_0 q^n \tag{14}$$

Now, substituting Eqs. (13) and (14) into Eq. (11), one obtains

$$\pi^0_{HS}=\sum_{n=1}^{m}\left[-\tfrac{1}{2}q^{n\gamma}K^n_0 q^n+F^{n\gamma}_0 q^n\right] \tag{15}$$

where

$$K^n_0=G^{n\gamma}_0\left(H^{n^{-1}}_0-H^{n^{-1}}_0 A^\gamma\left(AH^{n^{-1}}_0 A^\gamma\right)^{-1}AH^{n^{-1}}_0\right)G^n_0$$

denotes the element stiffness matrix of element n. Assembling Eq. (15) for $n=1,2,\cdots m$, π^0_{HS} becomes

$$\pi^0_{HS}=-\tfrac{1}{2}q^{*\gamma}K^*_0 q^*+F^{*\gamma}_0 q^* \tag{16}$$

where K^*_0, F^*_0, and q^* are the assembled global matrix of K^n_0, F^n_0, and q^n for $n=1,2,\cdots m$. Finally, the stationary condition of π^0_{HS} in Eq. (16) with respect to the global nodal displacements q^* yields

$$K^*_0 q^*=F^*_0 \tag{17}$$

Solving the system of simultaneous algebraic equations of Eq. (17), the global nodal displacements q^* and the deformation of the composite laminate are determined. Substituting the solutions of the global nodal displacements into Eqs. (14) and (6), the three-dimensional stresses $\hat{\sigma}^{0^i}$ of the entire composite structure are then computed.

B. Buckling Analysis

To describe the buckling of general composite laminates, the assumed hybrid-stress functional π_{HS} can be derived from the modified complementary energy principle as follows:

$$\pi_{HS}(\sigma^i;w^i_{,p};u^i)=\sum_{n=1}^{m}\left\{\sum_{i=1}^{k}\left[\int_{v^i_n}\left(\tfrac{1}{2}\sigma^{i\gamma}S^i\sigma^i+\tfrac{1}{2}w^{i\gamma}_{,p}\underset{\sim}{g}{}^i_p w^i_{,p}\right)\mathrm{d}v-\int_{\partial v^i_n}T^{i\gamma}u^i\,\mathrm{d}s+\int_{S^i_{\sigma_n}}\bar{T}^{i\gamma}u^i\,\mathrm{d}s\right]\right\}=\min \tag{18}$$

in which

$$w^i_{,p}=\begin{Bmatrix}w^i_{,x}\\ w^i_{,y}\end{Bmatrix},\qquad \underset{\sim}{g}{}^i_p=\begin{pmatrix}\sigma^i_{xx} & \sigma^i_{xy}\\ \sigma^i_{xy} & \sigma^i_{yy}\end{pmatrix} \tag{19}$$

and σ^i are the three-dimensional stresses, which are assumed such that the equilibrium conditions within each layer

$$\sigma^i_{xx,x}+\sigma^i_{xy,y}+\sigma^i_{xz,z}=0 \tag{20}$$

$$\sigma^i_{yx,x}+\sigma^i_{yy,y}+\sigma^i_{yz,z}=0 \tag{21}$$

$$(\sigma^i_{zx}+\sigma^i_{xx}w_{,x}+\sigma^i_{xy}w_{,y})_{,x}+(\sigma^i_{zy}+\sigma^i_{yx}w_{,x}+\sigma^i_{yy}w_{,y})_{,y}+(\sigma^i_{zz}+\sigma^i_{zx}w_{,x}+\sigma^i_{zy}w_{,y})_{,z}=0 \tag{22}$$

and the interlaminar traction reciprocity conditions are satisfied; the displacements u^i of the ith layer, which are measured from the state just prior to the occurrence of buckling; w is the component of u^i in z direction; x, y, and z are the Cartesian coordinate axes (see Fig. 1); and $\bar{T}^i$ is the prescribed tractions at $S^i_{\sigma_n}$ of the ith layer as buckling occurs. It is assumed that $\bar{T}^i$ vary neither in magnitude nor in direction during buckling.

In Eq. (18), σ^i includes σ^{0^i} and σ^{*i}. σ^{0^i} is the three-dimensional stresses at the state just prior to the occurrence of buckling whereas σ^{*i} denotes the incremental stresses at the occurrence of buckling. Since σ^{0^i} satisfies the equilibrium condition of the state prior to the occurrence of buckling and σ^{*i} is small as compared with σ^{0^i}, the functional π_{HS} in Eq. (18) may be reduced to the following form:

$$\pi_{HS}(\sigma^{*i};w^i_{,p};u^i)=\sum_{n=1}^{m}\left\{\sum_{i=1}^{k}\left[\int_{v^i_n}\left(\tfrac{1}{2}\sigma^{*i\gamma}S^i\sigma^{*i}+\tfrac{1}{2}w^{i\gamma}_{,p}\underset{\sim}{g}{}^{0^i}_p w^i_{,p}\right)\mathrm{d}v-\int_{\partial v^i_n}T^{*i\gamma}u^i\,\mathrm{d}s\right]\right\}=\min \tag{23}$$

in which

$$\underset{\sim}{g}{}^{0^i}_p=\begin{pmatrix}\sigma^{0^i}_{xx} & \sigma^{0^i}_{xy}\\ \sigma^{0^i}_{xy} & \sigma^{0^i}_{yy}\end{pmatrix} \tag{24}$$

and T^{*i} is the incremental boundary tractions for the ith layer at the occurrence of buckling.

If the prescribed tractions $\bar{T}^i$ for the buckling are assumed as μ times the prescribed traction $\bar{T}^{0^i}$ before the occurrence of buckling as shown in Eq. (1), the three-dimensional stresses σ^{0^i} are then equal to $\mu\hat{\sigma}^{0^i}$. μ is a constant. Equations (23) and (24) can be rewritten as

$$\pi_{HS}(\sigma^{*i};w^i_{,p};u^i)=\sum_{n=1}^{m}\left\{\sum_{i=1}^{k}\left[\int_{v^i_n}\left(\frac{1}{2}\sigma^{*i\gamma}S^i\sigma^{*i}+\frac{\mu}{2}w^{i\gamma}_{,p}\underset{\sim}{\hat{g}}{}^{0^i}_p w^i_{,p}\right)\mathrm{d}v-\int_{\partial v^i_n}T^{*i\gamma}u^i\,\mathrm{d}s\right]\right\}=\min \tag{25}$$

where

$$\underset{\approx}{\hat{\sigma}}_p^{0^i} = \begin{pmatrix} \hat{\sigma}_{xx}^{0^i} & \hat{\sigma}_{xy}^{0^i} \\ \hat{\sigma}_{xy}^{0^i} & \hat{\sigma}_{yy}^{0^i} \end{pmatrix} \tag{26}$$

The equilibrium conditions of Eqs. (20–22) may be also rewritten as

$$\sigma_{xx}^{*^i}{}_{,x} + \sigma_{xy}^{*^i}{}_{,y} + \sigma_{xz}^{*^i}{}_{,z} = 0 \tag{27}$$

$$\sigma_{yx}^{*^i}{}_{,x} + \sigma_{yy}^{*^i}{}_{,y} + \sigma_{yz}^{*^i}{}_{,z} = 0 \tag{28}$$

$$\left(\sigma_{xz}^{*^i} + \mu\hat{\sigma}_{xx}^{0^i} w_{,x} + \mu\hat{\sigma}_{xy}^{0^i} w_{,y}\right)_{,x} + \left(\sigma_{yz}^{*^i} + \mu\hat{\sigma}_{yx}^{0^i} w_{,x} + \mu\hat{\sigma}_{yy}^{0^i} w_{,y}\right)_{,y} + \left(\sigma_{zz}^{*^i} + \mu\hat{\sigma}_{zx}^{0^i} w_{,x} + \mu\hat{\sigma}_{zy}^{0^i} w_{,y}\right)_{,z} = 0 \tag{29}$$

In this case, the composite multilayer element is taken as that used for interlaminar stress analysis. The incremental interelement boundary displacements $\boldsymbol{u}^i$ are interpolated in terms of the generalized incremental nodal displacements $\boldsymbol{q}^i$ as

$$\boldsymbol{u}^i = L^i \boldsymbol{q}^i \tag{30}$$

Following the same procedure for assuming $\hat{\sigma}_{xx}^{0^i}$, $\hat{\sigma}_{xy}^{0^i}$, and $\hat{\sigma}_{yy}^{0^i}$, the incremental in-plane stresses in the ith layer can also be expressed in terms of parameters $\boldsymbol{\beta}$.

The assumed variables $w_{,x}^i$ and $w_{,y}^i$ in the ith layer of the nth element are expressed as

$$w_{,x}^i = \alpha_1 + x\alpha_2 + y\alpha_3 + x^2\alpha_4 + xy\alpha_5 + y^2\alpha_6$$

$$w_{,y}^i = \alpha_7 + x\alpha_8 + y\alpha_9 + x^2\alpha_{10} + xy\alpha_{11} + y^2\alpha_{12}$$

or in matrix form

$$\boldsymbol{w}_{,p}^i = P_1 \boldsymbol{\alpha} \tag{31}$$

Again, following similar procedures for obtaining $\hat{\sigma}_{zz}^{0^i}$, $\hat{\sigma}_{xz}^{0^i}$, and $\hat{\sigma}_{yz}^{0^i}$, the normal stress σ_{zz}^* and transverse shear stresses σ_{xz}^* and σ_{yz}^* can be computed from Eqs. (27–29) and Eq. (31). (Now, the three-dimensional stresses $\hat{\boldsymbol{\sigma}}^{0^i}$ are known.) The incremental three-dimensional stresses $\boldsymbol{\sigma}^{*^i}$ and boundary tractions $\boldsymbol{T}^{*^i}$ in the ith layer of the nth element are then expressed as

$$\boldsymbol{\sigma}^{*^i} = N_1^i \boldsymbol{\beta} + \mu N_2^i \boldsymbol{\alpha} \tag{32}$$

$$\boldsymbol{T}^{*^i} = R_1^i \boldsymbol{\beta} + \mu R_2^i \boldsymbol{\alpha} \tag{33}$$

Substituting Eqs. (30–33) into Eq. (25), the functional π_{HS} can be formulated as

$$\pi_{HS} = \sum_{n=1}^{m} \left[\sum_{i=1}^{k} \left(\frac{1}{2}\boldsymbol{\beta}^\gamma H_1^i \boldsymbol{\beta} + \mu\boldsymbol{\beta}^\gamma H_2^{i\gamma} \boldsymbol{\alpha} + \frac{\mu^2}{2}\boldsymbol{\alpha}^\gamma H_3^i \boldsymbol{\alpha} + \frac{\mu}{2}\boldsymbol{\alpha}^\gamma H_4^i \boldsymbol{\alpha} - \boldsymbol{\beta}^\gamma G_1^i \boldsymbol{q}^i - \mu\boldsymbol{\alpha}^\gamma G_2^i \boldsymbol{q}^i \right) \right] \tag{34}$$

where

$$H_1^i = \int_{v_n^i} N_1^{i\gamma} S^i N_1^i \, dv \tag{35}$$

$$H_2^i = \int_{v_n^i} N_2^{i\gamma} S^i N_1^i \, dv \tag{36}$$

$$H_3^i = \int_{v_n^i} N_2^{i\gamma} S^i N_2^i \, dv \tag{37}$$

$$H_4^i = \int_{v_n^i} P_1^\gamma \underset{\approx}{\hat{\sigma}}_p^{0^i} P_1 \, dv \tag{38}$$

$$G_1^i = \int_{\partial v_n^i} R_1^{i\gamma} L^i \, ds \tag{39}$$

$$G_2^i = \int_{\partial v_n^i} R_2^{i\gamma} L^i \, ds \tag{40}$$

After assembling the parameters in Eq. (34) for all layers, π_{HS} is found to be

$$\pi_{HS} = \sum_{n=1}^{m} \left[\frac{1}{2}\boldsymbol{\beta}^\gamma H_1^n \boldsymbol{\beta} + \mu\boldsymbol{\beta}^\gamma H_2^{n\gamma} \boldsymbol{\alpha} + \frac{\mu^2}{2}\boldsymbol{\alpha}^\gamma H_3^n \boldsymbol{\alpha} + \frac{\mu}{2}\boldsymbol{\alpha}^\gamma H_4^n \boldsymbol{\alpha} - \boldsymbol{\beta}^\gamma G_1^n \boldsymbol{q}^n - \mu\boldsymbol{\alpha}^\gamma G_2^n \boldsymbol{q}^n \right] \tag{41}$$

where H_1^n, H_2^n, H_3^n, H_4^n, G_1^n, G_2^n, and $\boldsymbol{q}^n$ are the corresponding assembled element matrices of H_1^i, H_2^i, H_3^i, H_4^i, G_1^i, G_2^i, and $\boldsymbol{q}^i, i = 1,2\cdots k$.

Since the incremental transverse shear stresses need to be free on the top surface of the laminate (say $A\boldsymbol{\beta} = \mathbf{0}$), the constraint condition can be satisfied via the Lagrangian multiplier technique. Hence, Eq. (41) becomes

$$\pi_{HS}(\boldsymbol{\beta};\boldsymbol{\alpha};\boldsymbol{q}^n;\lambda) = \sum_{n=1}^{m} \left[\frac{1}{2}\boldsymbol{\beta}^\gamma H_1^n \boldsymbol{\beta} + \mu\boldsymbol{\beta}^\gamma H_2^{n\gamma} \boldsymbol{\alpha} + \frac{\mu^2}{2}\boldsymbol{\alpha}^\gamma H_3^n \boldsymbol{\alpha} + \frac{\mu}{2}\boldsymbol{\alpha}^\gamma H_4^n \boldsymbol{\alpha} - \boldsymbol{\beta}^\gamma G_1^n \boldsymbol{q}^n - \mu\boldsymbol{\alpha}^\gamma G_2^n \boldsymbol{q}^n + \lambda^\gamma A\boldsymbol{\beta} \right] \tag{42}$$

From Eq. (10), the stationary condition of the functional π_{HS} in Eq. (42) with respect to $\boldsymbol{\beta}$ yields

$$\lambda = \left(AH_1^{n^{-1}}A^\gamma\right)^{-1} AH_1^{n^{-1}} G_1^n \boldsymbol{q}^n - \mu\left(AH_1^{n^{-1}}A^\gamma\right)^{-1} AH_1^{n^{-1}} H_2^{n\gamma}\boldsymbol{\alpha} \tag{43}$$

$$\boldsymbol{\beta} = D^{n^{-1}} G_1^n \boldsymbol{q}^n - \mu D^{n^{-1}} H_2^{n\gamma}\boldsymbol{\alpha} \tag{44}$$

where

$$D^{n^{-1}} = H_1^{n^{-1}} - H_1^{n^{-1}} A^\gamma \left(AH_1^{n^{-1}}A^\gamma\right)^{-1} AH_1^{n^{-1}}$$

Substituting Eqs. (43) and (44) into Eq. (42), the functional π_{HS} is rearranged as

$$\pi_{HS}(\boldsymbol{\alpha};\boldsymbol{q}^n) = \sum_{n=1}^{m} \left[-\frac{1}{2}\boldsymbol{q}^{n\gamma} G_1^{n\gamma} D^{n^{-1}} G_1^n \boldsymbol{q}^n + \mu\boldsymbol{\alpha}^\gamma H_2^n D^{n^{-1}} G_1^n \boldsymbol{q}^n - \frac{\mu^2}{2}\boldsymbol{\alpha}^\gamma H_2^n D^{n^{-1}} H_2^{n\gamma}\boldsymbol{\alpha} + \frac{\mu^2}{2}\boldsymbol{\alpha}^\gamma H_3^n \boldsymbol{\alpha} + \frac{\mu}{2}\boldsymbol{\alpha}^\gamma H_4^n \boldsymbol{\alpha} - \mu\boldsymbol{\alpha}^\gamma G_2^n \boldsymbol{q}^n \right] \tag{45}$$

Next, the stationary condition of the functional π_{HS} in Eq. (45) with respect to $\boldsymbol{\alpha}$ yields

$$\boldsymbol{\alpha} = -C^{n^{-1}}\left(H_2^n D^{n^{-1}} G_1^n - G_2^n\right)\boldsymbol{q}^n \tag{46}$$

where

$$C^n = \mu\left(H_3^n - H_2^n D^{n^{-1}} H_2^{n\gamma}\right) + H_4^n \tag{47}$$

In Eq. (47), since the first term of the right-hand side is small as compared with H_4^n, then $C^n = H_4^n$.

Now, substituting Eq. (46) into Eq. (45), one obtains

$$\pi_{HS} = \sum_{n=1}^{m} \left[-\tfrac{1}{2}\boldsymbol{q}^{n\gamma}(K^n + \mu K_\sigma^n)\boldsymbol{q}^n \right] \tag{48}$$

where

$$K^n = G_1^{n\gamma} D^{n^{-1}} G_1^n \tag{49}$$

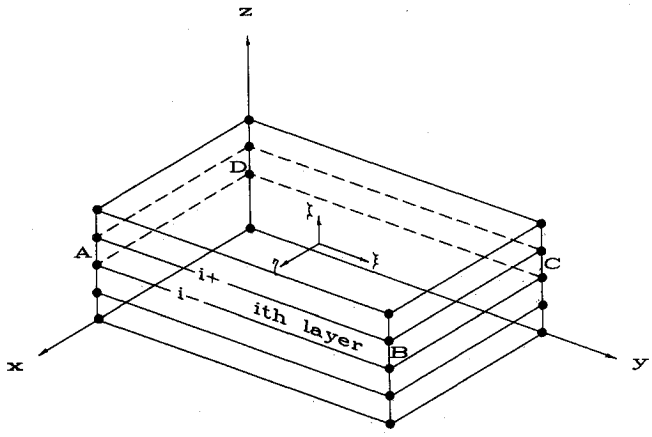

Fig. 1 Topology of multilayer element.

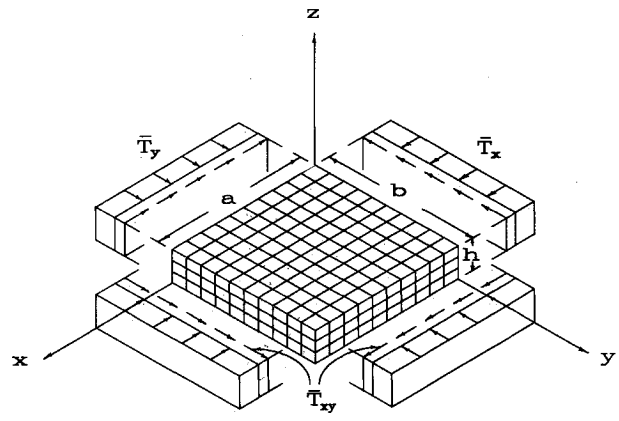

Fig. 2 Geometry and finite element mesh of a laminated plate.

$$K_\sigma^n = \left(H_2^n D^{n^{-1}} G_1^n - G_2^n\right)^\gamma C^{n^{-1}} \left(H_2^n D^{n^{-1}} G_1^n - G_2^n\right) \tag{50}$$

denote the bending stiffness matrix and the initial-stress stiffness matrix of the nth element, respectively. Assembling Eq. (48) for $n = 1,2,\cdots m$, π_{HS} can be rewritten as

$$\pi_{HS} = -\tfrac{1}{2}\, q^{*\gamma}(K^* + \mu K_\sigma^*) q^* \tag{51}$$

where K^*, K_σ^*, and q^* are the assembled global matrices of K^n, K_σ^n, and q^n for $n = 1,2,\cdots m$. As a result, the stationary condition of π_{HS} in Eq. (51) with respect to the global incremental nodal displacements q^* yields the relation

$$(K^* + \mu K_\sigma^*) q^* = \mathbf{0} \tag{52}$$

Solving the preceding eigenvalue problem, the eigenvalue μ which is physically the critical buckling load is then determined. It is noted that the corresponding eigenvector q^* only depicts the buckled shape instead of its magnitude.

The buckling analysis procedures for the general composite laminates can be summarized as follows. 1) Assuming an initial loading $\bar{P}$ that can be computed from the prescribed initial tractions $\bar{T}^{0^i}$ as shown in Eq. (1), calculate the distributions of the three-dimensional interlaminar stresses in the composite laminate which are treated as the initial stresses $\hat{\sigma}^{0^i}$ for buckling analysis. Loading $\bar{P}$ should be smaller than the critical buckling load. 2) Substitute the initial stresses $\hat{\sigma}^{0^i}$ into Eqs. (38), (47), and (50) and calculate the global initial-stress stiffness matrix K_σ^*. 3) Construct and solve Eq. (52) to obtain the smallest eigenvalue μ by the subspace iteration method.[15] The critical buckling load $\mu\bar{P}$ can be thus determined.

III. Element and Interpolation Function

The topology of the multilayer element devised in this work is shown in Fig. 1. The total number of nodes per element is $4\times(i+1)$ if the laminate consists of i layers, $i = 1,2,\cdots k$.

The interelement boundary displacements u^i for the ith layer for this element are expressed uniquely in terms of respective nodal displacements. Since $\epsilon_{zz} \simeq 0$, the transverse displacement through the thickness of the laminate is assumed as constant. Hence, for example, the components of u^i along the side surface A-B for ith layer as seen in Fig. 1 can be expressed as

$$u_\gamma^i = \tfrac{1}{4}\left[(1-\xi)(1-\zeta)\right] u_{\gamma A}^{i-} + \tfrac{1}{4}\left[(1+\xi)(1-\zeta)\right] u_{\gamma B}^{i-} + \tfrac{1}{4}\left[(1-\xi)(1+\zeta)\right] u_{\gamma A}^{i+} + \tfrac{1}{4}\left[(1+\xi)(1+\zeta)\right] u_{\gamma B}^{i+} \tag{53}$$

and

$$u_z^i = \tfrac{1}{2}(1-\xi) u_{z_A} + \tfrac{1}{2}(1+\xi) u_{z_B}$$

where $u_\gamma^i (\gamma = x,y)$ and u_z^i represent the in-plane displacements and transverse displacement at the side surface A-B of ith layer. The superscripts $i-$ and $i+$ denote the bottom and top surfaces of the ith layer, and ξ, ζ, and η are nondimensional local coordinates ($-1 \le \xi$, ζ and $\eta \le 1$). From Eq. (53), it is seen that the assumptions of in-plane displacements u_γ^i allow independent cross-sectional rotations of each layer. The total degree of freedoms per element are $8\times(i+1)+4$ if the laminate consists of i layers, $i = 1,2,\cdots k$. Hence, the interpolation matrix L^i in Eqs. (2) and (30) can be obtained.

The in-plane strain field in the ith layer is assumed as that of Chen and Hung.[13] The interpolation functions N_0^i in Eq. (6) and N_1^i and N_2^i in Eq. (32) for the three-dimensional stress field are thus derived. To avoid spurious kinematic modes of the element, the number of β chosen should obey the condition $b \le a + c$, where a, b, and c denote the number of independent parameters β, element nodal displacement q^i, and rigid-body modes, respectively.[16]

IV. Results and Discussion

To evaluate the validity and accuracy of the technique presented, a number of numerical examples are demonstrated. In all problems, the same material properties are considered for all layers and one of the following three materials is used:

Material 1: $E_L/E_T = 40$, $G_{LT}/E_T = 0.6$, $G_{TT}/E_T = 0.5$, $\nu_{LT} = \nu_{TT} = 0.25$

Material 2: $E_L/E_T = 40$, $G_{LT}/E_T = 0.6$, $G_{TT}/E_T = 0.5$, $\nu_{LT} = 0.25$, $\nu_{TT} = 0.49$

Material 3: $E_L/E_T = 40$, $G_{LT}/E_T = 0.5$, $G_{TT}/E_T = 0.2$, $\nu_{LT} = \nu_{TT} = 0.25$

where subscripts L and T represent the longitudinal and transverse direction of the lamina, respectively.

Table 1 Uniaxial buckling loads $\bar{T} = \bar{T}_x b^2/E_T h^2$ of simply supported symmetric cross-ply composite plates ($a/h = 10$; $a = b$)

Refs.	No. of layers	E_L/E_T = 20	30	40
CPT	3	19.7120	27.9360	36.1600
Noor[1]		15.0191	19.3040	22.8807
Putcha and Reddy[4]		15.3001	19.6752	23.3398
Khdeir and Librescu[7]		15.0320	19.0520	22.3120
Khdeir[8]		14.8900	18.8780	22.1210
Present		15.6804	19.5468	22.6980
CPT	5	19.7120	27.9360	36.1600
Noor[1]		15.6527	20.4663	24.5929
Putcha and Reddy[4]		16.0100	21.0023	25.3086
Khdeir and Librescu[7]		15.8620	20.6440	24.7270
Khdeir[8]		15.7830	20.5780	24.6760
Present		16.6308	21.1844	25.0644

Table 2 Biaxial buckling loads $\bar{T}=\bar{T}_y b^2/E_T h^2$ of the symmetric cross-ply (0 deg/90 deg/0 deg) laminated plates with one pair of opposite edges simply supported ($\bar{T}_x=\bar{T}_y$; $a=b$; material 2)

Refs.	b/h	SS[a]	SC	CC[b]	FF[c]	FS
CPT		14.7040	23.3810	34.4540	2.0250	2.5960
Khdeir and Librescu[7]	2	1.4650	1.4680	1.4720	0.9470	1.0850
Khdeir[8]		1.5080	1.6160	1.7900	0.8550	1.0060
Present		1.4789	1.5044	1.5537	0.7643	1.0961
CPT		14.7040	23.3810	34.4540	2.0250	2.5960
Khdeir and Librescu[7]	5	5.5260	5.8880	6.1630	1.7130	2.1140
Khdeir[8]		5.4640	5.7810	6.2190	1.6560	2.0400
Present		5.5231	5.7079	5.9780	1.5234	1.8943
CPT		14.7040	23.3810	34.4540	2.0250	2.5960
Khdeir and Librescu[7]	10	10.2590	11.6340	13.2880	1.9370	2.4490
Khdeir[8]		9.9750	11.5340	13.4830	1.9180	2.4200
Present		10.2921	11.7590	13.5452	1.8480	2.1965
CPT		14.7040	23.3810	34.4540	2.0250	2.5960
Khdeir and Librescu[7]	15	12.2260	15.4470	19.5260	1.9850	2.5260
Khdeir[8]		12.0500	15.3750	19.7060	1.9760	2.5100
Present		12.6892	15.9932	20.2006	1.9456	2.4252

[a]S: simply supported. [b]C: clamped. [c]F: free.

Table 3 Buckling loads $\bar{T}=\bar{T}_y b^2/E_T h^2$ of the symmetric cross-ply (0 deg/90 deg/0 deg) laminated plates with one pair of opposite edges simply supported ($b/h=10$; material 2)

Load	Refs.	b/a	SS[b]	SC	CC[c]	FF[d]	FS
$\bar{T}_x=\bar{T}_y$	Khdeir and Librescu[7]	2[a]	21.203	22.021	23.456	1.937	3.947
	Khdeir[8]		20.422	22.369	24.873	1.917	3.886
	Present		21.954	23.236	25.153	1.694	3.396
	Khdeir and Librescu[7]	1	10.259	11.634	13.288	1.937	2.449
	Khdeir[8]		9.975	11.534	13.483	1.918	2.420
	Present		10.292	11.759	13.545	1.848	2.197
$\bar{T}_x=0$ $\bar{T}_y\neq 0$	Khdeir and Librescu[7]	2[a]	29.200	29.804	30.819	1.925	4.046
	Khdeir[8]		27.375	29.271	30.846	1.907	4.004
	Present		29.037	29.911	30.931	1.981	4.286
	Khdeir and Librescu[7]	1	12.824	14.585	16.649	1.925	2.472
	Khdeir[8]		12.469	14.568	17.029	1.907	2.448
	Present		12.624	14.480	16.664	1.966	2.506

[a]8×14 meshes are adopted for full laminated plate. [b]S: simply supported. [c]C: clamped. [d]F: free.

Table 4 Effect of fiber orientation on the uniaxial buckling load $\bar{T}=\bar{T}_x b^2/E_T h^2$ of pin-supported angle-ply $(+\theta/-\theta)$ laminate ($b/h=20$; $a=b$; material 3)

	Fiber orientation, θ				
Sources	0 deg	30 deg	45 deg	75 deg	90 deg
Present	31.0414	20.2027	19.9243	12.7115	12.7368
CPT[17]	35.8310	20.4410	21.7090	12.9150	13.1320

Table 5 Effect of fiber orientation on the biaxial buckling load $\bar{T}=\bar{T}_x b^2/E_T h^2$ of angle-ply laminates ($b/h=10$; $a=b$; $\bar{T}_x=\bar{T}_y$; material 1)

No. of layers	θ, deg	SSSS	CCCC	CFCF
2	30	13.8763	14.6641	4.6549
	45	11.7974	14.8188	5.7771
3	30	17.7273	28.3406	4.8032
	45	16.4125	28.1935	5.7723

Table 6 Effect of number of layers on the shear buckling load $\bar{T}=\bar{T}_{xy} b^2/E_T h^2$ of angle-ply laminates (30 deg/ -30 deg/30 deg/ $\cdots$; $b/h=10$; $a=b$; $\bar{T}_x=\bar{T}_y=0$; material 1)

No. of layers	SSSS	SCSC	CCCC	CFCF
2	21.3122	23.8373	24.3581	12.4024
3	23.5388	26.9259	28.4803	7.1591

The geometry and finite element mesh taken in this work are shown in Fig. 2. Unless otherwise stated, 10×10 multilayer elements are adopted for the full laminated plate.

The influences of the modulus ratio and number of layers on the dimensionless uniaxial buckling loads $\bar{T}=\bar{T}_x b^2/E_T h^2$ for simply supported symmetric cross-ply laminates are tabulated in Table 1. The material properties are the same as those of material 1 except that the modulus ratios are taken. Because of symmetry, only a quadrant of the plate is modeled and 8×8 multilayer elements are chosen. Good correlations between the present computed results and referenced solutions[1,4,7,8] reveal the high accuracy of the present technique. In addition, as the modulus ratio increases, the present results are closer to the solutions[1] obtained by three-dimensional elasticity as compared with those computed by Putcha and Reddy[4] using mixed finite element method. Tables 2 and 3 show the various effects of thickness ratio, edge conditions, and aspect ratio on the dimensionless buckling loads $\bar{T}=\bar{T}_y b^2/E_T h^2$ of symmetric cross-ply (0 deg/90 deg/0 deg) laminated plates with one pair

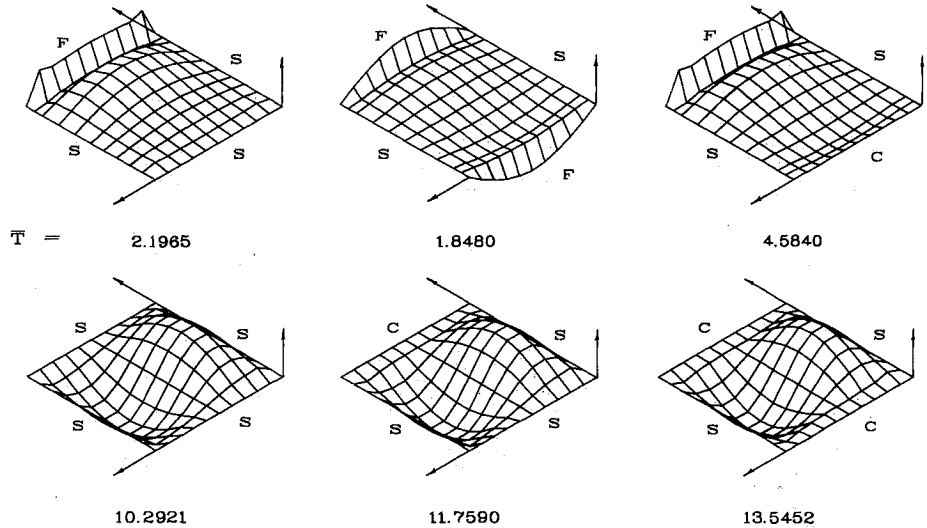

Fig. 3 Biaxial-buckled shapes of symmetric cross-ply laminates (0 deg/90 deg/0 deg) for various edge conditions ($a=b$; $b/h=10$; $\bar{T}=\bar{T}_y b^2/E_T h^2$).

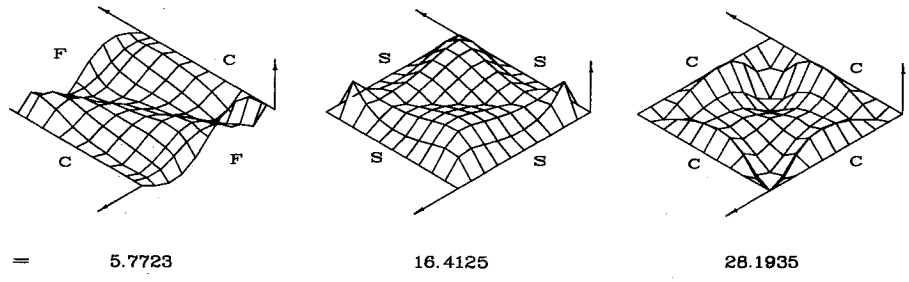

Fig. 4 Biaxial-buckled shapes of symmetric angle-ply laminates (45 deg/−45 deg/45 deg) for various edge conditions ($a=b$; $b/h=10$; $\bar{T}=\bar{T}_x b^2/E_T h^2$).

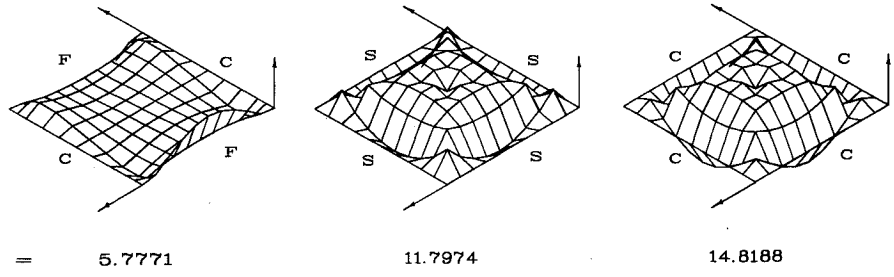

Fig. 5 Biaxial-buckled shapes of antisymmetric angle-ply laminates (45 deg/−45 deg) for various edge conditions ($a=b$; $b/h=10$; $\bar{T}=\bar{T}_x b^2/E_T h^2$).

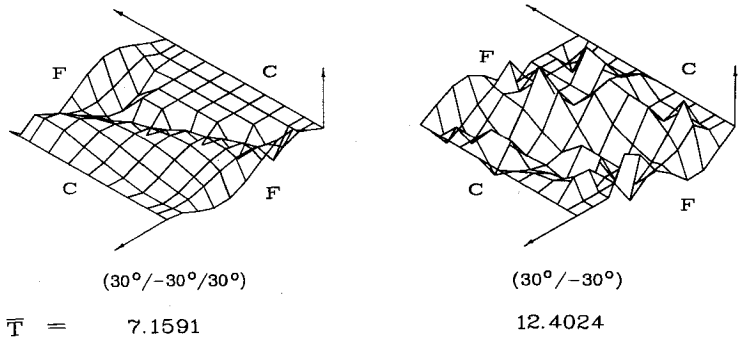

Fig. 6 Shear-buckled shapes of symmetric (30 deg/−30 deg/30 deg) and antisymmetric (30 deg/−30 deg) angle-ply for CFCF edge condition ($a=b$; $b/h=10$; $\bar{T}=\bar{T}_{xy} b^2/E_T h^2$).

of opposite edges simply supported at $y=0$ and $y=b$. Again, good results show the high accuracy and versatility of the present technique. Table 4 displays the effect of fiber orientations on the dimensionless uniaxial buckling load for a two-layered antisymmetric angle-ply laminated plate with pin-supported edge conditions. The solutions of Jones et al.[17] by the classical plate theory are also shown for comparison purposes. In Table 5, results are presented for studying the effect of fiber orientations on the biaxial buckling load of the angle-ply laminated plates with different number of layers and four edge conditions. It is seen that the biaxial buckling loads for CFCF plates have no obvious difference between three-layered symmetric and two-layered antisymmetric angle-ply laminates. For other plates with SSSS or CCCC conditions, as would be expected, the buckling loads of antisymmetric laminates are much smaller than those of symmetric laminates. Table 6 shows the effect of the number of layers on the shear buckling load of laminated plates having various edge conditions. It is interesting to note that the two-layered CFCF plate has higher shear buckling load as compared with three-layered plate. Figure 3 shows the biaxial-buckled shapes of symmetric cross-ply laminates having various edge conditions. Figures 4 and 5 display the biaxial-buckled shapes for symmetric (45 deg/−45 deg/45 deg) and antisymmetric (45 deg/−45 deg) angle-ply laminates with different boundary conditions, respectively. The shear-buckled shapes of symmetric (30 deg/−30 deg/30 deg) and antisymmetric (30 deg/−30 deg) angle-ply CFCF plates are shown in Fig. 6. An irregular shear-buckled shape can be seen for the antisymmetric angle-ply plate.

V. Conclusions

An accurate and efficient multilayer element together with the hybrid-stress finite element models formulated have been successfully demonstrated for the buckling analysis of general composite laminates having various edge conditions under in-plane stress system. The effects of fiber orientations, aspect ratios, stacking sequences, and thickness of laminates on the buckling loads and buckled shapes are also investigated. Good results show the high accuracy and versatility of the present technique. Without using the composite shear-correction factors, since the analysis model is derived based on a three-dimensional viewpoint, the program as developed can be further employed to deal with more realistic composite structures, such as a composite laminate with a hole, etc.

References

[1]Noor, A. K., "Stability of Multilayered Composite Plates," *Fibre Science Technology,* Vol. 8, 1975, pp. 81–89.

[2]Turvey, G. J., "Biaxial Buckling of Moderately Thick Laminated Plates," *Journal of Strain Analysis,* Vol. 12, April 1977, pp. 89–95.

[3]Reddy, J. N., and Phan, N. D., "Stability and Vibration of Isotropic, Orthotropic, and Laminated Plates According to a Higher-Order Shear-Deformation Theory," *Journal of Sound and Vibration,* Vol. 98, Jan. 1985, pp. 157–170.

[4]Putcha, N. S., and Reddy, J. N., "Stability and Natural Vibration Analysis of Laminated Plates by Using a Mixed Element Based on a Refined Plate Theory," *Journal of Sound and Vibration,* Vol. 104, Jan. 1986, pp. 285–300.

[5]Reddy, J. N., "A Simple Higher-Order Theory for Laminated Composite Plates," *Journal of Applied Mechanics,* Vol. 51, Dec. 1984, pp. 745–752.

[6]Librescu, L., and Khdeir, A. A., "Analysis of Symmetric Cross-Ply Laminated Elastic Plates Using a Higher-Order Theory: Pt. I—Stress and Displacement," *Composite Structures,* Vol. 9, 1988, pp. 189–213.

[7]Khdeir, A. A., and Librescu, L., "Analysis of Symmetric Cross-Ply Laminated Elastic Plates Using a Higher-Order Theory: Pt. II—Buckling and Free Vibration," *Composite Structures,* Vol. 9, 1988, pp. 259–277.

[8]Khdeir, A. A., "Free Vibration and Buckling of Symmetric Cross-Ply Laminated Plates by an Exact Method," *Journal of Sound and Vibration,* Vol. 126, Nov. 1988, pp. 447–461.

[9]Singh, G., and Sadasiva Rao, Y. V. K., "Stability of Thick Angle-Ply Composite Plates," *Computers and Structures,* Vol. 29, 1988, pp. 317–322.

[10]Dawe, D. J., and Craig, T. J., "The Vibration and Stability of Symmetrically Laminated Composite Rectangular Plates Subjected to In-Plane Stresses," *Composite Structures,* Vol. 5, 1986, pp. 281–307.

[11]Whitney, J. M., "Curvature Effects in the Buckling of Symmetrically Laminated Rectangular Plates with Transverse Shear Deformation," *Composite Structures,* Vol. 8, 1987, pp. 85–103.

[12]Baharlou, B., and Leissa, A. W., "Vibration and Buckling of Generally Laminated Composite Plates with Arbitrary Edge Conditions," *International Journal of Mechanical Sciences,* Vol. 29, 1987, pp. 545, 555.

[13]Chen, W. H., and Hung, T. F., "Three-Dimensional Interlaminar Stress Analysis at Free Edges of Composite Laminate," *Computers and Structures,* Vol. 32, 1989, pp. 1275–1286.

[14]Pian, T. H. H., and Tong, P., "Finite-Element Methods in Continuum Mechanics," *Advances in Applied Mechanics,* Vol. 12, edited by C. S. Yih, Academic, New York, 1972, pp. 2–53.

[15]Bathe, K.-J., *Finite-Element Procedures in Engineering Analysis,* Prentice-Hall, Englewood Cliffs, NJ, 1982, pp. 672–694.

[16]Nishioka, T., and Atluri, S. N., "Assumed Stress Finite-Element Analysis of Through-Cracks in Angle-Ply Laminates," *AIAA Journal,* Vol. 18, Sept. 1980, pp. 1125–1132.

[17]Jones, R. M., Morgan, H. S., and Whitney, J. M., "Buckling and Vibration of Antisymmetrically Laminated Angle-Ply Rectangular Plates," *Journal of Applied Mechanics,* Vol. 40, Dec. 1973, pp. 1143, 1144.